nature cell biology

Oct4 kinetics predict cell lineage patterning in the early mammalian embryo

Nicolas Plachta[1], Tobias Bollenbach[2,3], Shirley Pease[1], Scott E. Fraser[1] and Periklis Pantazis[1,4]

Transcription factors are central to sustaining pluripotency, yet little is known about transcription factor dynamics in defining pluripotency in the early mammalian embryo. Here, we establish a fluorescence decay after photoactivation (FDAP) assay to quantitatively study the kinetic behaviour of Oct4, a key transcription factor controlling pre-implantation development in the mouse embryo. FDAP measurements reveal that each cell in a developing embryo shows one of two distinct Oct4 kinetics, before there are any morphologically distinguishable differences or outward signs of lineage patterning. The differences revealed by FDAP are due to differences in the accessibility of Oct4 to its DNA binding sites in the nucleus. Lineage tracing of the cells in the two distinct sub-populations demonstrates that the Oct4 kinetics predict lineages of the early embryo. Cells with slower Oct4 kinetics are more likely to give rise to the pluripotent cell lineage that contributes to the inner cell mass. Those with faster Oct4 kinetics contribute mostly to the extra-embryonic lineage. Our findings identify Oct4 kinetics, rather than differences in total transcription factor expression levels, as a predictive measure of developmental cell lineage patterning in the early mouse embryo.

At present, it remains strongly debated how early cells in the mammalian embryo acquire the first developmental differences that can predict lineage patterning[1,2]. In human and mouse, cell lineage patterning is first evident after the 8-cell embryo undergoes compaction[3,4]. Some cells divide in a symmetric manner, contributing two daughter cells to the outside region of the embryo, whereas others divide asymmetrically, contributing one daughter cell to the outside and another to the inside region. Cells allocated to the inside region during the 8- to 16-cell transition ('inside cells') give rise to the pluripotent cell lineage that eventually contributes to the inner cell mass (ICM), and subsequently to the epiblast and primitive endoderm. Those allocated to the outside region ('outside cells') may divide symmetrically to contribute to the extra-embryonic trophectoderm[1,2] or asymmetrically to contribute one cell to the trophectoderm and another to the primitive endoderm[5]. Although the difference becomes manifest only at the 16-cell stage, some studies suggest that cells are predisposed to contribute more inside or outside cells at the 4-cell stage. In these studies, certain cleavage patterns have been shown to predict developmental differences[6], possibly reflecting intrinsic differences between the cells that result from epigenetic modifications[7]. Contrary to this model, others have argued that lineage allocation is decided stochastically by cell interactions only at the 16- to 32-cell stage[8–10]. Thus, a reproducible cellular and molecular difference that defines the establishment of the pluripotent or extra-embryonic lineage is strongly debated.

The transcription factor Oct4 (also known as Pou5f1) has been shown to have a central role in the patterning of the pluripotent cell lineage[8,11–16] and is thus a good candidate for establishing developmental differences among early cells. Embryos lacking the *Oct4* gene fail to form the inside cell lineage[13] and sustained Oct4 overexpression can reprogram various somatic cell types into pluripotency, either in combination with other transcription factors[17] or by itself[18,19]. However, Oct4 is expressed by all cells in the embryo at heterogeneous levels between the 1-cell to late blastocyst stage, and it seems that its expression level is not predictive of cell lineage patterning[8]. Beyond protein expression levels, the biological activity of most transcription factors relies directly on their kinetic behaviours in individual cells[20,21]. For instance, fluorescence time-lapse analyses in cultured mammalian cells have revealed distinct kinetics of oscillatory transcription factors that can control gene expression[22,23]. So far however, the lack of tools needed to follow transcription factor kinetics in complex geometrical systems has precluded studies within embryos.

RESULTS

Quantitative imaging of Oct4–paGFP kinetics using FDAP

To examine whether the kinetic behaviour of Oct4 predicts cell lineage patterning in live embryos, we studied Oct4 quantitatively in four dimensions (x, y, z and time) using photoactivatable green fluorescent protein (paGFP). This modified version of GFP shows a ~100-fold increase in 488-nm-emitted fluorescence after activation with ~400 nm light[24]; previous work in *Drosophila melanogaster* reported photoactivation of paGFP with three-dimensional precision using multiphoton excitation[25]. To express paGFP in live mouse embryos we microinjected cytoplasmic

[1]Division of Biology, California Institute of Technology, 1200 E. California Blvd, Pasadena, CA 91125, USA. [2]Department of Systems Biology, Harvard Medical School, 200 Longwood Avenue, Boston, MA 02115, USA.[3]Present address: Institute of Science and Technology Austria, Am Campus 1, A-3400 Klosterneuburg, Austria. [4]Correspondence should be addressed to P.P. (email: pantazis@caltech.edu)

Received 09 September 2010; accepted 07 November 2010; published online 23 January 2011; corrected online 28 January 2011; DOI: 10.1038/ncb2154

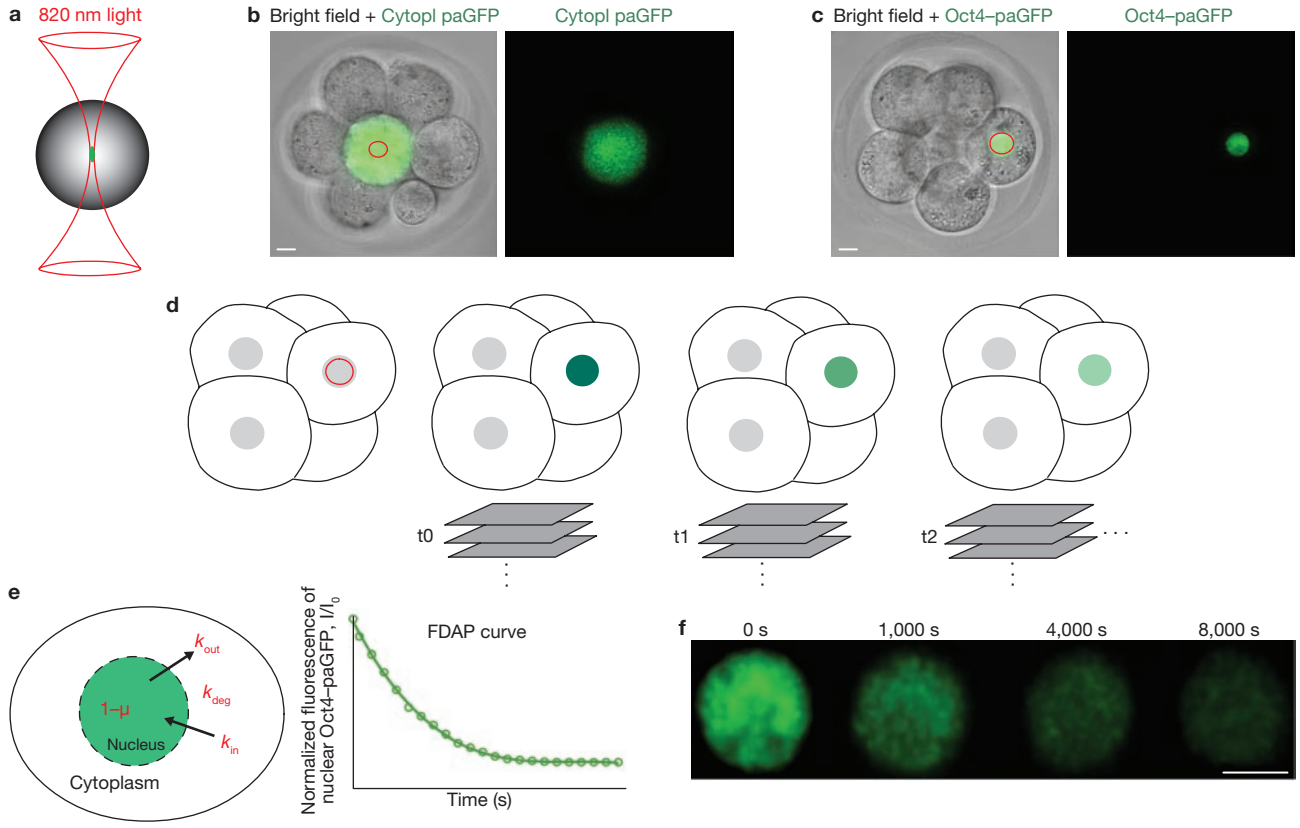

Figure 1 Selective photoactivation in live mouse embryos allows imaging of Oct4–paGFP kinetic behaviours. (**a**) Schematic diagram of photoactivation of paGFP (green) within a defined volume (grey sphere) using 820 nm light. (**b**) Photoactivation of cytoplasmic (cytopl) paGFP within a small ROI (red circle) localized to one cell of a live 8-cell stage embryo. Following photoactivation paGFP fluorescence spreads throughout the cytoplasm of the photoactivated cell. (**c**) Photoactivation of Oct4–paGFP within a ROI localized to a single cell nucleus of the embryo. (**d**) Schematic representation of the FDAP assay. Following photoactivation within a single cell nucleus, Oct4–paGFP fluorescence (green) is tracked in four dimensions with confocal time-lapse imaging. (**e**) FDAP analysis. The photoactivated Oct4–paGFP (green in simplified model, left) is initially in the nucleus and then moves from the nucleus to the cytoplasm. The parameters k_{in}, k_{out} and k_{deg} are the rates of Oct4–paGFP import into the nucleus from the cytoplasm, export from the nucleus to the cytoplasm, and the rate of overall degradation within the entire cell, respectively. $1–\mu$ denotes the immobile fraction of nuclear Oct4-paGFP. Theoretical time development of the average Oct4-paGFP fluorescence profile (I/I_0; normalized to the initial level of nuclear Oct4–paGFP fluorescence) in a FDAP experiment. (**f**) Representative FDAP time-lapse images showing Oct4–paGFP fluorescence over time in the cell nucleus photoactivated in **c**. Scale bar, 10 μm.

paGFP RNA into the 1-cell stage and allowed the embryos to develop to the 8-cell stage. Using ultrashort laser light pulses (~200 fs; 820 nm; Fig. 1a), photoactivation of a small region of interest (ROI) caused a ~15-fold increase of fluorescence, which rapidly spread throughout the cytoplasm and caused no photodamage (Fig. 1b). Photoactivation of cytoplasmic paGFP in fixed embryos demonstrates the spatial confinement of the multiphoton activation (Supplementary Fig. S1).

To enable us to evaluate the kinetics of Oct4 in the living embryo, we generated an Oct4–paGFP fusion protein. This fluorescently labelled transcription factor localizes predominantly in the nucleus and retains its function, as has been previously demonstrated using an Oct4–GFP fusion[26]. We microinjected the linear Oct4–paGFP plasmid into one cell of the 2-cell stage embryo, together with RNA encoding histone H2B fused to red fluorescent protein (H2B–RFP), which labelled chromatin and allowed us to follow the lineage of the injected cell through division. Photoactivation was later performed within labelled daughters of the injected cell (Fig. 1c and Supplementary Movie 1). Immunolabelling using Oct4 antibodies and quantification of average fluorescence intensities revealed that the total levels of Oct4 in H2B–RFP labelled nuclei were within the physiological range of the endogenous Oct4 protein (Supplementary information, Supplementary Fig. S2a–c). Thus, a fraction of functional Oct4–paGFP molecules can be photoactivated and imaged in the cell nucleus of mouse embryos using multiphoton excitation.

We designed a fluorescence decay after photoactivation (FDAP) assay, consisting of photoactivation of Oct4–paGFP in the nucleus and monitoring of its movement out of the nucleus using time-lapse confocal imaging (Fig. 1d, e, Supplementary Movie 2). During imaging, embryos were maintained under constant 37 °C and 5% CO_2 conditions and *z*-planes were acquired every 5 min for 4 h (Fig. 1f). In a typical FDAP experiment, we photoactivated Oct4–paGFP in up to three cell nuclei per embryo at the same time and quantified the subsequent decrease of fluorescence intensity in each nucleus over time (Fig. 1d, e). For analysis, the average fluorescence intensity was quantified in a circular ROI covering 95% of the photoactivated nucleus (see Supplementary information). Quantification of fluorescence was also performed in H2B–RFP labelled nuclei of non-activated neighbour cells so that the background fluorescence intensity could be subtracted. We verified that photobleaching is negligible during imaging (Supplementary Fig. S3a). To obtain the

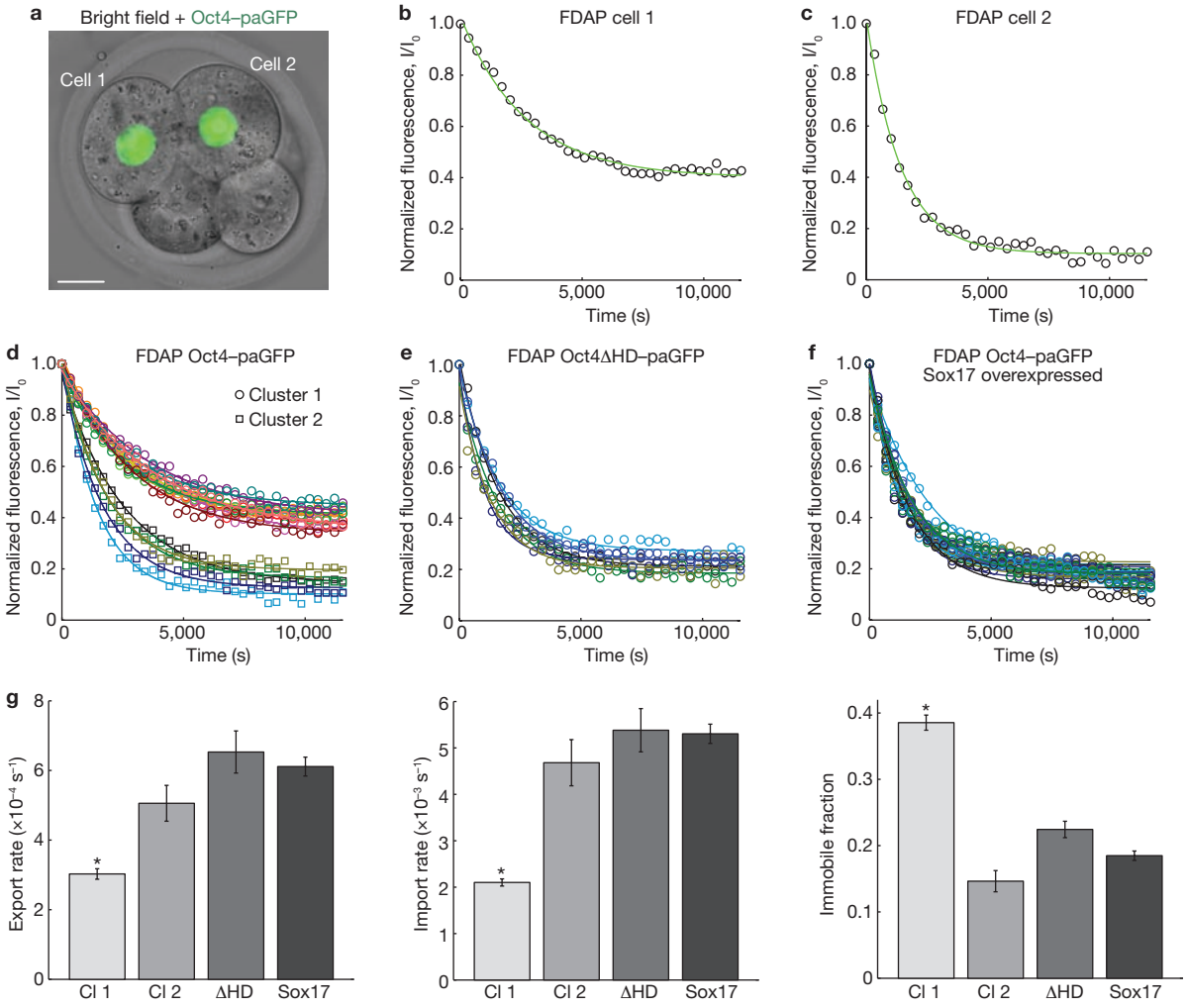

Figure 2 Oct4–paGFP kinetic behaviours identify two cell populations in the mouse embryo. (**a**) Examples of a pre-compaction embryo showing two photoactivated cell nuclei. Scale bar corresponds to 15 μm. (**b**, **c**) FDAP curves show average fluorescence intensity of Oct4–paGFP within the cell nuclei photoactivated in **a** over time. Green lines are exponential fits to fluorescence data. (**d**) FDAP curves for Oct4–paGFP obtained from several cell nuclei of pre-compaction embryos combining 4-cell stage and 8-cell stage data. Cells show two distinct kinetic behaviours, divided into clusters 1 and 2. (**e**) FDAP curves for Oct4ΔHD–paGFP at pre-compaction stages. (**f**) FDAP curves for Oct4–paGFP in cells that overexpress Sox17 at pre-compaction stages. (**g**) Quantification of Oct4–paGFP nuclear export, import and immobile fraction. Cl 1, cluster 1; Cl 2, cluster 2; ΔHD, Oct4ΔHD–paGFP; Sox17, Sox17 overexpressed. In **d**–**g**, Cl 1, $n = 11$; Cl 2, $n = 5$; ΔHD, $n = 6$; Sox 17, $n = 15$. Asterisks show statistically significant differences (export, $P < 0.015$; import, $P < 0.006$, immobile $P < 1 \times 10^{-5}$). Error bars show standard deviations.

degradation rate of the Oct4 fusion protein (see Supplementary information), we photoactivated Oct4–paGFP in the entire cell (Supplementary Fig. S3b). We found that the rates of degradation were similar among cells in all the developmental stages analysed in our study (0.14 ± 0.01 h^{-1}), corresponding to a half-life of approximately 5 h, which is similar to the 6–8 h half-life of Oct4 determined biochemically in cultured cells[27]. Finally, we (1) verified efficient photoactivation of Oct4–paGFP (Supplementary Fig. S3c), (2) confirmed that the average fluorescence intensity of photoactivated Oct4–paGFP is linearly related to the concentration of molecules (Supplementary Fig. S3d), and (3) ensured even light penetration in mouse embryos to avoid misestimation of the amount of total photoactivated fluorescence (Supplementary Fig. S3e).

Two distinct Oct4–paGFP kinetics before cell lineage patterning

To investigate Oct4–paGFP kinetics in the embryo before the inside and outside cell lineages are anatomically defined, we photoactivated Oct4–paGFP in the nucleus (Fig. 2a) and measured its kinetic behaviours in 4-cell and 8-cell stage embryos (Fig. 2b–d). From the resulting time-dependent FDAP profiles, we extracted in single cells of developing mouse embryos the rates of Oct4–paGFP nuclear export and import and the immobile fraction[28] (see Supplementary information). The rates of Oct4–paGFP nuclear export and import agree well with values for facilitated nucleocytoplasmic transport rather than passive diffusion[29]. At both developmental stages, we found that cells fell into two clusters with distinct Oct4–paGFP kinetic behaviours (Fig. 2b–d and Supplementary Fig. S4). Cells of cluster 1 had lower rates of export and import and a larger immobile fraction than cells of cluster 2 (Fig. 2g and Table 1). Each cell cluster comprised about half of the cells analysed at the 4-cell and 8-cell stage (Table 1) and the two clusters were morphologically indistinguishable at these developmental stages. Furthermore, the stereotypical kinetic behaviours exhibited by cells in the two cell clusters were unrelated to the initial intensity of Oct4–paGFP fluorescence within

Table 1 Summary of Oct4 kinetic parameters analysed

	Nuclear export k_{out} ($\times 10^{-3}$ s^{-1})	Nuclear import k_{in} ($\times 10^{-3}$ s^{-1})	Immobile fraction $(1-\mu)$	n	R^2
Oct4-paGFP pre-compaction (cluster 1)	0.28 ± 0.01	1.89 ± 0.07	0.40 ± 0.01	19 (7 at 4-cell stage, 12 at 8-cell stage)	0.988 ± 0.001
Oct4-paGFP pre-compaction (cluster 2)	0.50 ± 0.02	4.58 ± 0.21	0.15 ± 0.01	12 (5 at 4-cell stage, 7 at 8-cell stage)	0.985 ± 0.002
Oct4-paGFP post-compaction (inside)	0.22 ± 0.02	1.63 ± 0.10	0.37 ± 0.03	9	0.985 ± 0.002
Oct4-paGFP post-compaction (outside)	0.42 ± 0.03	4.00 ± 0.28	0.12 ± 0.02	6	0.987 ± 0.001
Oct4ΔHD-paGFP	0.65 ± 0.06	5.38 ± 0.47	0.22 ± 0.01	6	0.980 ± 0.006
Oct4-paGFP, Sox17 overexpressed	0.61 ± 0.03	5.30 ± 0.21	0.18 ± 0.01	15	0.974 ± 0.003
H2B–paGFP	0.22 ± 0.01	0.75 ± 0.04	0.72 ± 0.03	3	0.952 ± 0.011
NLS_{Oct4}–paGFP	0.87 ± 0.12	7.62 ± 1.27	0.18 ± 0.03	5	0.966 ± 0.006
paGFP–Sox2	0.21 ± 0.03	1.19 ± 0.15	0.51 ± 0.02	8	0.977 ± 0.003

For all values the mean and the standard error are reported. n indicates the number of experiments considered for each experimental condition. The agreement between the experimental data and the theoretical curves used to derive the kinetic parameters is described by R^2 values. The parameters k_{out} and k_{in} are the rates of Oct4–paGFP export from the nucleus to the cytoplasm, and import into the nucleus from the cytoplasm, respectively. The parameter $1-\mu$ denotes the immobile fraction of nuclear Oct4-paGFP.

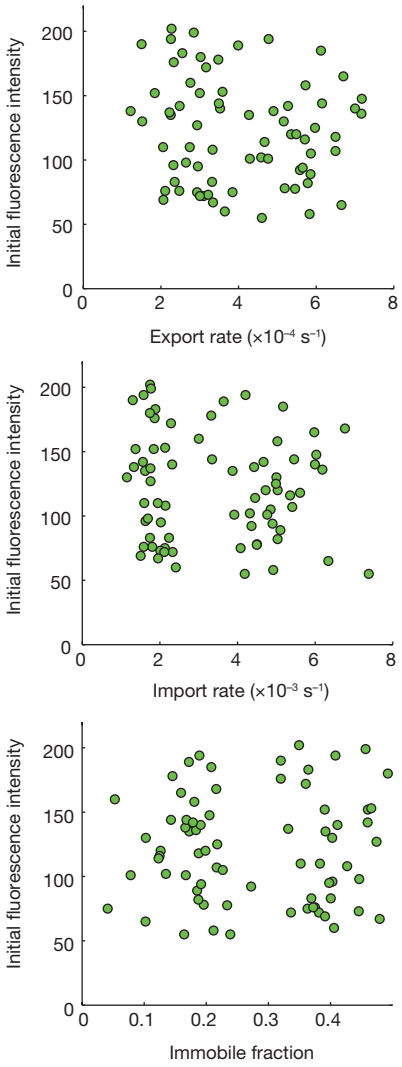

Figure 3 Oct4–paGFP kinetics are uncorrelated to total fluorescence in the cell nucleus. Relation between the initial level of Oct4–paGFP fluorescence within the cell nucleus and the export rate, import rate and immobile fraction values obtained using FDAP analysis for single cells from Fig. 2d. The initial values of Oct4–paGFP fluorescence are unrelated to any of the kinetic parameters.

their cell nuclei (Fig. 3). Together, these results show that Oct4–paGFP kinetics identify cryptic differences between two cell populations that are morphologically indistinguishable before cell lineage patterning becomes evident (during the 8- to 16-cell transition).

To determine whether the presence of distinct kinetics were specific to paGFP when fused to Oct4, we tested a situation in which paGFP was instead fused to H2B, a structural protein with known high retention within the nucleus[30], or in which paGFP bore only the nuclear localization signal of Oct4[26] (NLS_{Oct4}) lacking any known specificity for binding to DNA or proteins. As expected, the FDAP profile of H2B–paGFP was markedly different from that of NLS_{Oct4}–paGFP, with the latter showing higher rates of export and import and a smaller immobile fraction (Supplementary Fig. S3f, g and Table 1). Importantly, the results from both paGFP fusions were uniform in kinetics, with no sign of the clustering of kinetics revealed for the Oct4–paGFP fusion. We then asked whether Sox2, another transcription factor present in all cell nuclei of the embryo before lineage allocation[31], exhibits distinct kinetic behaviours. Unlike that of Oct4–paGFP, the FDAP profile of paGFP–Sox2 revealed a uniform kinetic behaviour at the 4- to 8-cell stage, and showed no clustering of its kinetics (Supplementary Fig. S3h and Table 1).

Distinct Oct4–paGFP kinetics result from differences in access to DNA binding sites

The higher immobile fraction of cluster 1 suggested that the two stereotypical Oct4–paGFP kinetic behaviours are caused by a different accessibility of the transcription factor to its binding sites in the nucleus. Transcription factor binding to DNA has been shown to be a major contributor to transcription factor kinetics inside cells[20,32]. We explored this by using a modified form of Oct4–paGFP that lacks the homeodomain region required for DNA binding (Oct4ΔHD–paGFP)[33]. The Oct4ΔHD–paGFP protein showed high rates of export and import and a low immobile fraction in all cells (Fig. 2e, g and Table 1), with values similar to those obtained with Oct4–paGFP in cells of cluster 2 (Fig. 2d, g). Thus, mutating Oct4 so that it interacts less well with DNA results in uniform and fast kinetics, suggesting that the clustering of the kinetics results from differences in access to DNA binding sites.

If the slower kinetics and higher immobile fraction resulted from Oct4–DNA interactions, then blocking DNA binding with an excess of another transcription factor should eliminate cluster 1. We tested this by overexpressing Sox17, a transcription factor recently shown to

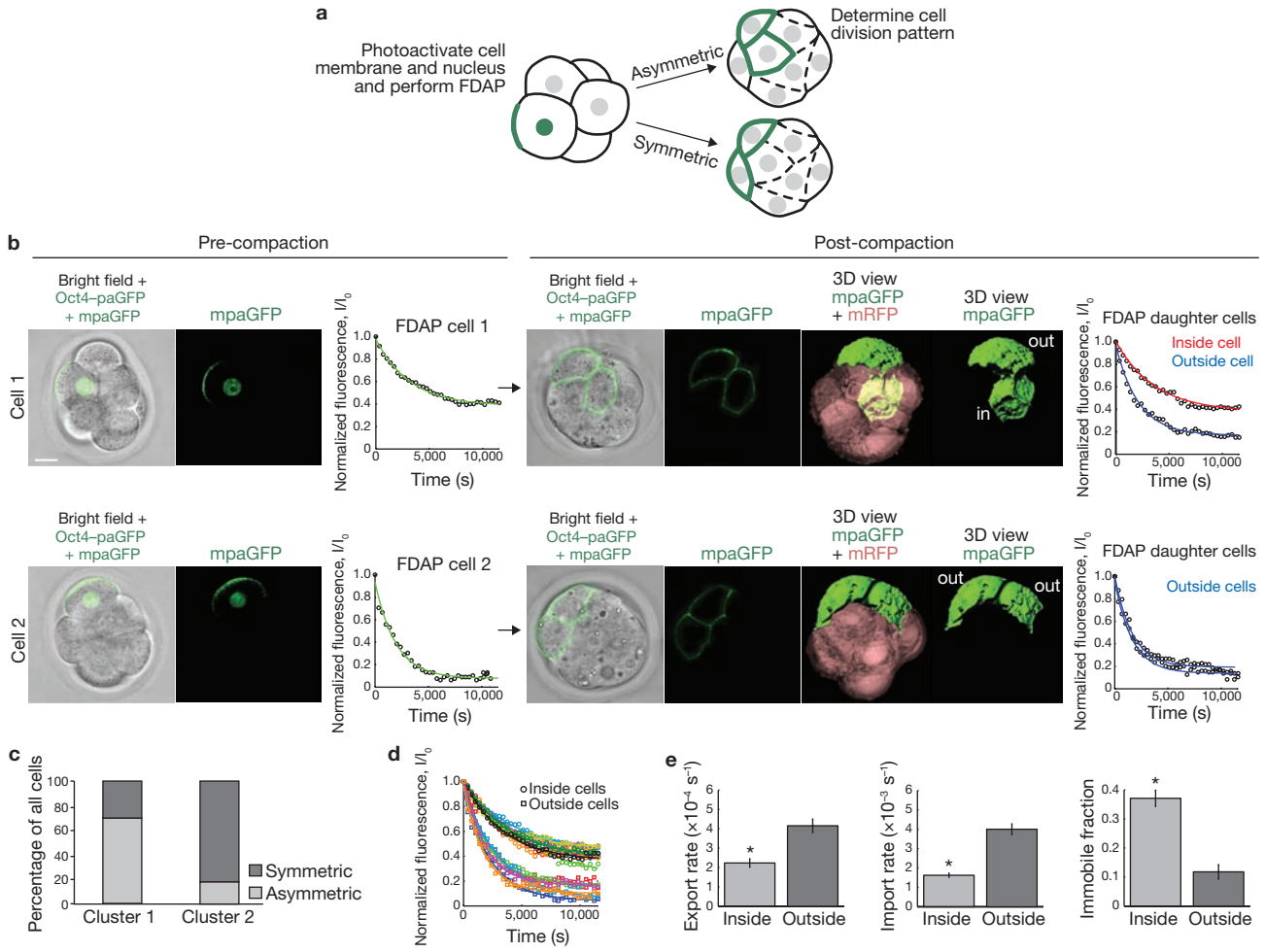

Figure 4 Oct4–paGFP kinetics predict patterning of inside and outside cells. (**a**) Schematic representation of the experimental strategy used. Following FDAP analysis and photoactivation of a membrane-targeted paGFP, embryos undergo compaction and the pattern of cell division is determined. (**b**) Examples of two pre-compaction embryos (left panels) show Oct4–paGFP fluorescence following photoactivation of single cell nuclei, and mpaGFP fluorescence following photoactivation of part of the membrane. The FDAP curves show the distinct Oct4–paGFP kinetic behaviours in each cell. Following compaction and division (right panels), cell 1 (top row) divided asymmetrically, generating one inside and one outside cell. Cell 2 (lower row) divided symmetrically, generating two outside cells. Surface rendered three-dimensional views confirm that the inside cell is buried within the embryo whereas outside cells have part of their surface exposed to the outer region. A membrane-targeted RFP (pink) marks half of the cells in these embryos. The FDAP curves on the right show the distinct Oct4–paGFP kinetic behaviours in each daughter cell of the original photoactivated cell. Scale bar, 15 μm. (**c**) Quantification of symmetric and asymmetric divisions undertaken following compaction by cells that showed the FDAP profiles of clusters 1 and 2 at pre-compaction stages. (**d**) FDAP curves show Oct4–paGFP kinetic behaviours in several inside and outside cells at post-compaction stages. (**e**) Quantification of Oct4–paGFP nuclear export, import and immobile fraction. Asterisks show statistical significant differences (export, $P = 0.0012$; import, $P = 1.4737 \times 10^{-4}$, immobile $P = 1.4154 \times 10^{-5}$). Error bars show standard deviations. In **d**, **e**, inside cells, $n = 9$; outside cells, $n = 6$.

compete for several of the same promoter sequences to which transcription factors classically associated with the pluripotent state bind[34]. Sox17 overexpression resulted in high rates of Oct4–paGFP export and import and a low immobile fraction (Fig. 2f, g and Table 1), making all cells show kinetics similar to those of Oct4ΔHD–paGFP (Fig. 2e) and to Oct4–paGFP in cells of cluster 2 (Fig. 2d). Taken together, the loss of cluster 1 in the rates of Oct4–paGFP motion suggests that the clustering is due to the accessibility of saturable (defined) DNA binding sites for Oct4 in some nuclei.

Oct4–paGFP kinetics predict lineage patterning

The presence of distinct Oct4–paGFP kinetic behaviours during pre-compaction stages (4- to 8-cell) raised the question of whether these kinetic differences predict events of embryonic patterning. To address this, we performed FDAP analyses to determine Oct4–paGFP kinetics in an individual cell, and then traced the progeny of that cell by photoactivating a lipid-modified paGFP (mpaGFP) on the cell's surface (Fig. 4a, b). Cells labelled in this way before compaction at the 8-cell stage were followed to determine whether they divide symmetrically, contributing daughter cells only to the outside lineage, or asymmetrically, contributing daughter cells to the outside and inside lineages, after the embryo had undergone compaction at the 16- to 32-cell stage[1,2]. We distinguished inside from outside cells by their position and morphology as described previously[35]: inside cells localized within the embryo; outside cells had part of their external surface area exposed to the surrounding zona pellucida. Cells of cluster 1, showing low rates of export and import and a large immobile fraction

Table 2 Summary of cell division patterns analysed

	Asymmetric (%)	Symmetric (%)	*n*	*P*-value
Cluster 1	70.6	29.4	17	0.0035
Cluster 2	17.6	82.4	17	0.0955
Sox17 overexpressed	0	100	7	0.0464

Percentage of cells of cluster 1, cluster 2, and Sox17 overexpression undergoing asymmetric and symmetric divisions following compaction, respectively. *n* indicates the number of experiments considered for each experimental condition. *P*-values are based on a one-sided binomial test with probability of asymmetric division of 0.355 (corresponding to the average fraction of asymmetric divisions in embryos at the 8-cell stage[5]).

at pre-compaction stages, underwent more asymmetric than symmetric divisions (70.6% asymmetric; $n = 12$ inside and 22 outside daughter cells generated from 17 photoactivated cells; Fig. 4b, c and Table 2). By contrast, cells of cluster 2, showing high rates of export and import and a small immobile fraction at pre-compaction stages, underwent mostly symmetric divisions (82.4% symmetric; $n = 3$ inside cells and 31 outside daughter cells generated from 17 photoactivated cells; Fig. 4b, c and Table 2).

In line with these results and supporting a causal role for the differences of Oct4 engagement, cells overexpressing Sox17, which blocks Oct4 engagement (showing Oct4–paGFP kinetic behaviours similar to cells of cluster 2), underwent only symmetric divisions. Sox17 overexpressing cells contributed all their progeny to the outside lineage ($n = 0$ inside and 14 outside daughter cells generated from 7 photoactivated cells; Table 2). Thus, cells of cluster 1 are the main progenitor source for the inside lineage, contributing over 4-fold more daughter cells to the pluripotent lineage than cells of cluster 2.

Oct4–paGFP kinetics correlate with the position of cells to the inside and outside lineage

Finally, we asked whether the stereotypical Oct4–paGFP kinetics observed before compaction (Fig. 2d) are maintained in inside and outside cells at the 16- to 32-cell stage. FDAP analyses at these stages revealed that inside cells showed slower Oct4–paGFP kinetics and a larger immobile fraction than outside cells (Fig. 4d, e and Table 1). The Oct4–paGFP kinetic behaviours of inside and outside cells were directly comparable to those of cells of cluster 1 and cluster 2, respectively, measured at pre-compaction stages (Fig. 2d, g and Table 1). This implies that outside daughter cells generated by symmetric divisions of cluster 2 cells as well as inside daughter cells generated by asymmetric divisions of cluster 1 cells maintain the same Oct4–paGFP kinetics as their progenitor cells. Only outside daughter cells (after asymmetric divisions taken by the majority of cells of cluster 1) adopt kinetics characteristic of the extra-embryonic cell lineage (Fig. 4b, right panels). Hence, Oct4–paGFP kinetics are not stochastic in the post-compacted embryo, but correlate with the position of cells to the inside and outside lineage. The significant differences in the probability of the generation of inside and outside daughter cells predicted by the distinct Oct4–paGFP kinetics agree well with recent lineage tracing studies describing the allocation of these two lineages[5].

DISCUSSION

Our quantitative characterization of Oct4–paGFP kinetics provides a tool for predicting pluripotency in the early mammalian embryo. Regardless of the biochemistry underlying the kinetic parameters described here, our results identify developmental heterogeneities based on the differential kinetic behaviour of a transcription factor before any clear signs of lineage patterning become visible (Fig. 5). Before compaction, cells show distinct but stereotypical rates of Oct4–paGFP kinetics (Fig. 2), revealing cryptic differences between two morphologically indistinguishable cell populations. The differences in Oct4–paGFP motion are due to differences between cells in the accessibility of the DNA binding sites for Oct4 in some nuclei. It will be important to assess in the future whether and how the distinct Oct4–paGFP kinetics reported here relate to previous demonstrations of cell heterogeneity in the early embryo. These include, for example, the order and orientation of cell divisions[2] and the levels of proteins involved in epigenetic modifications[7], which have been described at the 4-cell stage, as well as the subcellular distribution of the transcription factor Cdx2 (ref. 5).

Competing for Oct4 binding sites by Sox17 overexpression causes all cells to show fast transport and small immobile fraction of Oct4–paGFP. Given that overexpression of Sox17 in our experiments results in cells that exclusively give rise to the extra-embryonic lineage of the mouse embryo, our results suggest that cells fated to the pluripotent cell lineage of the ICM depend on functional engagement of Oct4 with its target sites in the DNA. This is in line with the large number of Oct4 target genes found in the genome of cultured embryonic stem cells and with the ability of Oct4 to interact with other transcription factors associated with pluripotent chromatin[11,12].

In conclusion, our work shows that measuring the levels of regulatory proteins in fixed or living specimens cannot necessarily capture developmental heterogeneities. The distinct kinetic behaviours we find for Oct4–paGFP are unrelated to the initial levels of Oct4–paGFP fluorescence within cell nuclei, suggesting that the difference is independent of transcription factor protein expression levels within the cell. Similarly, recent studies in cultured cells and *Xenopus* embryos have shown that transcriptional activity is not predicted by the absolute proteins levels[36,37]. Our FDAP assay has provided early information about the fate of undifferentiated cells in the early mouse embryo, suggesting it offers an important tool for assessing the developmental potential of somatic cells reprogrammed into pluripotency[17]. □

ACKNOWLEDGEMENTS

We especially thank Juan Silva and John Earle for excellent technical support with mouse embryo work. We also thank H. Schöler, J. Lippincott-Schwartz, G. Patterson and Li-Jin Chew for constructs. N.P. is supported by California Institute for Regenerative Medicine (CIRM), European Molecular Biology Organization (EMBO) and Swiss National Science Foundation (SNF), fellowships. T.B. was supported by the Alexander von Humboldt foundation. P.P. is supported by the German Science Foundation (DFG). This work was supported by the Beckman Institute and Biological Imaging Center at the California Institute of Technology and by the NHGRI Center of Excellence in Genomic Science grant P50HG004071.

AUTHOR CONTRIBUTIONS

T.B. performed the quantitative analysis. S.P. performed microinjections into mouse embryos. N.P., S.E.F. and P.P. designed and N.P. and P.P. carried out all other experiments.

COMPETING FINANCIAL INTERESTS

The authors declare that they have no competing financial interests.

Published online at http://www.nature.com/naturecellbiology/
Reprints and permissions information is available online at http://npg.nature.com/reprintsandpermissions/

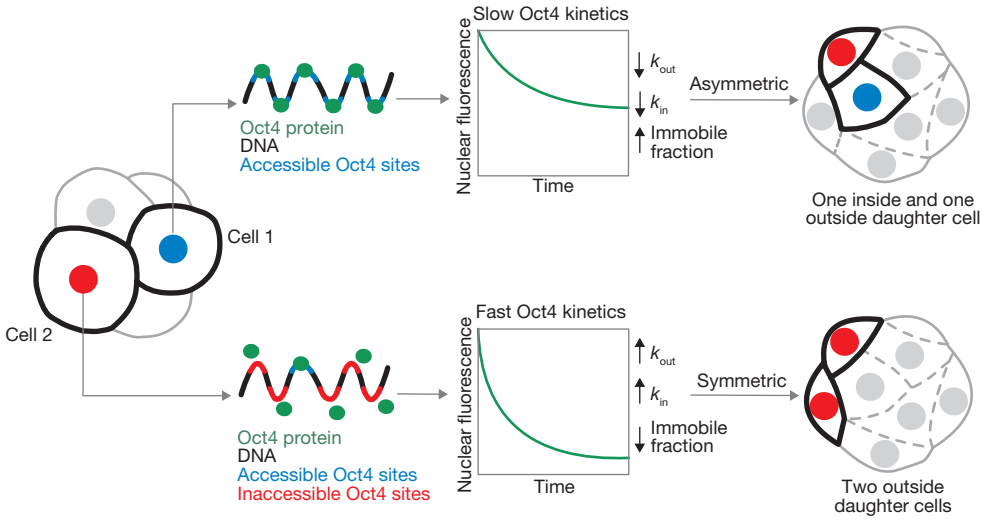

Figure 5. Schematic illustration of Oct4–paGFP kinetics and cell lineage allocation in the early mouse embryo. Different accessibility of Oct4 DNA binding sites among cells, possibly due to a differential chromatin structure, the presence of an excess of another factor that blocks access or the absence of a cofactor required for high-affinity binding, results in segregation of Oct4–paGFP kinetic properties before lineage allocation. Cells with slower kinetics and a large immobile fraction divide more frequently in an asymmetric manner during the 8- to 16-cell transition, contributing more cells to the pluripotent cell lineage, whereas cells with faster kinetics and a small immobile fraction contribute more cells to the extra-embryonic lineage through symmetric divisions.

1. Rossant, J. & Tam, P. P. Blastocyst lineage formation, early embryonic asymmetries and axis patterning in the mouse. *Development* **136**, 701–713 (2009).
2. Zernicka-Goetz, M., Morris, S. A. & Bruce, A. W. Making a firm decision: multifaceted regulation of cell fate in the early mouse embryo. *Nat. Rev. Genet.* **10**, 467–477 (2009).
3. Tarkowski, A. K. & Wroblewska, J. Development of blastomeres of mouse eggs isolated at the 4- and 8-cell stage. *J. Embryol. Exp. Morphol.* **18**, 155–180 (1967).
4. Ziomek, C. A. & Johnson, M. H. Cell surface interaction induces polarization of mouse 8-cell blastomeres at compaction. *Cell* **21**, 935–942 (1980).
5. Morris, S. A., *et al.* Origin and formation of the first two distinct cell types of the inner cell mass in the mouse embryo. *Proc. Natl Acad. Sci. USA* **107**, 6364–6369 (2010).
6. Zernicka-Goetz, M. Cleavage pattern and emerging asymmetry of the mouse embryo. *Nat. Rev. Mol. Cell Biol.* **6**, 919–928 (2005).
7. Torres-Padilla, M. E., Parfitt, D. E., Kouzarides, T. & Zernicka-Goetz, M. Histone arginine methylation regulates pluripotency in the early mouse embryo. *Nature* **445**, 214–218 (2007).
8. Dietrich, J. E. & Hiiragi, T. Stochastic patterning in the mouse pre-implantation embryo. *Development* **134**, 4219–4231 (2007).
9. Kurotaki, Y., Hatta, K., Nakao, K., Nabeshima, Y. & Fujimori, T. Blastocyst axis is specified independently of early cell lineage but aligns with the ZP shape. *Science* **316**, 719–723 (2007).
10. Motosugi, N., Bauer, T., Polanski, Z., Solter, D. & Hiiragi, T. Polarity of the mouse embryo is established at blastocyst and is not prepatterned. *Genes Dev.* **19**, 1081–1092 (2005).
11. Boyer, L. A., Mathur, D. & Jaenisch, R. Molecular control of pluripotency. *Curr. Opin. Genet. Dev.* **16**, 455–462 (2006).
12. Remenyi, A., Scholer, H. R. & Wilmanns, M. Combinatorial control of gene expression. *Nat. Struct. Mol. Biol.* **11**, 812–815 (2004).
13. Nichols, J., *et al.* Formation of pluripotent stem cells in the mammalian embryo depends on the POU transcription factor Oct4. *Cell* **95**, 379–391 (1998).
14. Rosner, M. H., *et al.* A POU-domain transcription factor in early stem cells and germ cells of the mammalian embryo. *Nature* **345**, 686–692 (1990).
15. Scholer, H. R., Dressler, G. R., Balling, R., Rohdewohld, H. & Gruss, P. Oct-4: a germline-specific transcription factor mapping to the mouse t-complex. *EMBO J.* **9**, 2185–2195 (1990).
16. Scholer, H. R., Ruppert, S., Suzuki, N., Chowdhury, K. & Gruss, P. New type of POU domain in germ line-specific protein Oct-4. *Nature* **344**, 435–439 (1990).
17. Takahashi, K. & Yamanaka, S. Induction of pluripotent stem cells from mouse embryonic and adult fibroblast cultures by defined factors. *Cell* **126**, 663–676 (2006).
18. Kim, J. B., *et al.* Oct4-induced pluripotency in adult neural stem cells. *Cell* **136**, 411–419 (2009).
19. Kim, J. B., *et al.* Direct reprogramming of human neural stem cells by OCT4. *Nature* **461**, 649–643 (2009).
20. Hager, G. L., McNally, J. G. & Misteli, T. Transcription dynamics. *Mol. Cell* **35**, 741–753 (2009).
21. Phair, R. D., *et al.* Global nature of dynamic protein–chromatin interactions in vivo: three-dimensional genome scanning and dynamic interaction networks of chromatin proteins. *Mol. Cell Biol.* **24**, 6393–6402 (2004).
22. Nelson, D. E., *et al.* Oscillations in NF-κB signaling control the dynamics of gene expression. *Science* **306**, 704–708 (2004).
23. Lahav, G., *et al.* Dynamics of the p53-Mdm2 feedback loop in individual cells. *Nat. Genet.* **36**, 147–150 (2004).
24. Patterson, G. H. & Lippincott-Schwartz, J. A photoactivatable GFP for selective photolabeling of proteins and cells. *Science* **297**, 1873–1877 (2002).
25. Pantazis, P. & Gonzalez-Gaitan, M. Localized multiphoton photoactivation of paGFP in *Drosophila* wing imaginal discs. *J. Biomed. Opt.* **12**, 044004 (2007).
26. Pan, G., Qin, B., Liu, N., Scholer, H. R. & Pei, D. Identification of a nuclear localization signal in OCT4 and generation of a dominant negative mutant by its ablation. *J. Biol. Chem.* **279**, 37013–37020 (2004).
27. Wei, F., Scholer, H. R. & Atchison, M. L. Sumoylation of Oct4 enhances its stability, DNA binding, and transactivation. *J. Biol. Chem.* **282**, 21551–21560 (2007).
28. Dudu, V., *et al.* Postsynaptic mad signaling at the *Drosophila* neuromuscular junction. *Curr. Biol.* **16**, 625–635 (2006).
29. Gorlich, D. & Kutay, U. Transport between the cell nucleus and the cytoplasm. *Annu. Rev. Cell Dev. Biol.* **15**, 607–660 (1999).
30. Wolffe, A. P. Centromeric chromatin. Histone deviants. *Curr. Biol.* **5**, 452–454 (1995).
31. Avilion, A. A., *et al.* Multipotent cell lineages in early mouse development depend on SOX2 function. *Genes Dev.* **17**, 126–140 (2003).
32. Elf, J., Li, G. W. & Xie, X. S. Probing transcription factor dynamics at the single-molecule level in a living cell. *Science* **316**, 1191–1194 (2007).
33. Remenyi, A., *et al.* Crystal structure of a POU/HMG/DNA ternary complex suggests differential assembly of Oct4 and Sox2 on two enhancers. *Genes Dev.* **17**, 2048–2059 (2003).
34. Niakan, K. K., *et al.* Sox17 promotes differentiation in mouse embryonic stem cells by directly regulating extraembryonic gene expression and indirectly antagonizing self-renewal. *Genes Dev.* **24**, 312–326 (2010).
35. Johnson, M. H. & Ziomek, C. A. Induction of polarity in mouse 8-cell blastomeres: specificity, geometry, and stability. *J. Cell Biol.* **91**, 303–308 (1981).
36. Cohen-Saidon, C., Cohen, A. A., Sigal, A., Liron, Y. & Alon, U. Dynamics and variability of ERK2 response to EGF in individual living cells. *Mol. Cell* **36**, 885–893 (2009).
37. Goentoro, L. & Kirschner, M. W. Evidence that fold-change, and not absolute level, of β-catenin dictates Wnt signaling. *Mol. Cell* **36**, 872–884 (2009).

DOI: 10.1038/ncb2154

METHODS

DNA constructs. To express photoactivatable Oct4 in mouse embryos, we engineered a construct (CAG::Oct4–paGFP) in which transcription of Oct4 fused to photoactivatable GFP is driven by the compound CAG promoter. CAG contains the chicken actin promoter, minimum cytomegalovirus (CMV) enhancer, and a large synthetic intron. Here, the mouse Oct4 open reading frame (ORF; provided by H. Schöler, Max-Planck Institute for Molecular Biomedicine, Münster, Germany), was cloned in-frame and upstream of the monomeric paGFP ORF (provided by J. Lippincott-Schwartz and G. Patterson, NIH, Bethesda, USA) and downstream of the CAG promoter, which drives constitutive expression in mouse embryos[38].

To express photoactivatable histone H2B, we engineered a similar construct (CAG::H2B–paGFP) in which the human H2B ORF was cloned downstream of the CAG promoter and in-frame upstream of the paGFP ORF.

To express photoactivatable Sox2, we engineered a construct (CAG::paGFP–Sox2) in which the mouse Sox2 ORF was cloned downstream of the CAG promoter and in-frame downstream of the paGFP ORF. This fluorescently labelled transcription factor is similar to a GFP-Sox2 fusion protein previously shown to retain its function[39] and to show a predominant nuclear localization[40].

The CAG::Oct4–paGFP, CAG::H2B–paGFP and CAG::paGFP–Sox2 constructs were linearized and microinjected at 2 ng/µl concentration into one cell of the 2-cell stage embryo. An *H2B–RFP* RNA (20 ng/µl) was co-injected to label the chromatin in the progeny of the injected cell. The FDAP assays for Oct4–paGFP, H2B–paGFP and paGFP–Sox2 were performed using the same imaging conditions. To rule out the possibility that the CAG promoter used to drive expression in our experiments influences the kinetic parameters described in our study, we performed the same experiments using RNA encoding Oct4–paGFP. For this we engineered a plasmid to synthesize *Oct4–paGFP* RNA and microinjected the RNA directly into the cell cytoplasm of one cell at the 2-cell stage, as described above for the DNA construct. In these experiments we found no correlation between the kinetic behaviour of Oct4–paGFP and the concentration of RNA microinjected (20 and 40 ng/µl). The results of Oct4–paGFP kinetic behaviours obtained using RNA were similar to those obtained using the DNA construct.

To generate CAG::NLS_{Oct4}–paGFP (NLS_{Oct4}), a sequence containing the nuclear localization signal of Oct4 (amino acids 198–233) was amplified from the mouse Oct4 ORF and cloned downstream of the CAG promoter and in-frame upstream of the paGFP ORF. CAG::Oct4ΔHD–paGFP was generated by amplifying a truncated region of the mouse Oct4 ORF (amino acids 1–233) lacking the homeodomain region and cloned downstream of the CAG promoter and in-frame upstream of the paGFP ORF.

To mark the cell surface of single cells of the embryo, we engineered constructs to synthesize RNA encoding a lipid-modified form of monomeric paGFP (mpaGFP) and RFP (mRFP). This myristoylated and palmitoylated modification targets the fluorescent proteins to the inner leaflet of the plasma membrane as previously described[41] (Fig. 4). The mpaGFP did not contribute to fluorescence in the cell nucleus in experiments in which only this RNA was microinjected (data not shown). To determine the position of photoactivated cells following cell division in relation to other cells in the embryo, we co-injected the *mRFP* RNA (30 ng/µl) that labelled the surface of all the cells injected. Three-dimensional reconstructions were obtained using a surface-rendering tool of the Imaris (Bitplane AG) software (Fig. 4b) that enabled us to determine whether cells had their entire surface buried inside the embryo (inside cells) or had part of their surface exposed to the outside zona pellucida (outside cells).

To photoactivate paGFP in the cytoplasm of fixed embryos (Supplementary Fig. S1) we engineered a construct to synthesize RNA encoding an untagged form of paGFP.

To overexpress Sox17, we synthesized *Sox17* RNA using a construct provided by L.-J. Chew (George Washington University, Washington DC, USA) previously described[42] and injected the RNA at 50 ng/µl into 2-cell stage embryos. Sox17 protein localized predominantly in the nuclei (Supplementary Fig. S5).

Ambion-Applied Biosystems kits were used to synthesize RNA and Qiagen (RNAeasy) kits were used for RNA purification.

Microinjection, *ex utero* culture and imaging of pre-implantation mouse embryos. C57/Bl6 wild-type females at 21 days of age were superovulated by hormone priming and then mated to FVB males. The superovulation regime called for 5 iu of pregnant mare serum gonadotropin given intraperitoneally and 5 iu of human chorionic gonadotrophin, given 48 h later, immediately before mating. Mated females were euthanized by CO_2 asphyxiation following the recommendations of the Panel of Euthanasia of the American Veterinary Association and the Institutional Animal Care and Use Committee at the California Institute of Technology. Embryos at the 1- or 2-cell stage were obtained by flushing oviducts with M2 medium (Millipore MR-015-D) and were cultured at 37 °C and 5% CO_2 in KSOM+AA medium (Millipore MR-106-D) covered by oil (Sigma, M8410). DNA and RNA constructs were diluted in pro-nuclear injection buffer (5mM Tris at pH 7.4, 5mM NaCl and 0.1 mM EDTA, in embryo tested water, Sigma W1503) and 0.5–1 pl was microinjected into the nucleus of one blastomere only, following standard protocols for pro-nuclear injection of zygotes. Embryos were then cultured inside Lab-Tek (Nunc) chambers at 37 °C and 5% CO_2. Embryos developed normally to hatched blastocyst stage in these chambers, both inside a standard cell incubator or in an incubator adapted to our Zeiss 510 laser scanning microscope that maintains 37 °C, 5% CO_2 and balanced pH. We systematically excluded from our analyses embryos showing signs of aberrant development due to *ex utero* culture (20–30% of all embryos). We analysed one to three cell nuclei per embryo and more than 50 embryos in total. Cells in the pre-implantation embryo divide every 12–24 h. In our experiments some cells underwent normal mitosis after photoactivation while we were imaging them. This indicates that the cells were healthy and that the photoactivation and imaging conditions did not interfere with their cell cycle. However, we excluded dividing cells from our kinetic analyses and focused only on cells at the G2 phase of the cell cycle, which is significantly longer than the G1/S phase and can be assessed by the volume of the cell nucleus (G1 cell nuclei are about half the volume of G2 cell nuclei; data not shown). We also excluded from our analyses cells from embryos that did not develop normally, which we assessed by returning embryos to the cell incubator and allowing them to develop to the early blastocyst stage (3.5 days post coitum (dpc)). Throughout our studies we used a LD C-APO 40 x/1.1 Zeiss objective. Multiphoton 820 nm excitation light was used for photoactivation of regions of interest (ROIs) and 488 nm and 563 nm light were used for imaging. For experiments using cytoplasmic paGFP (Supplementary Fig. S1), embryos were microinjected at the 1-cell stage with *paGFP* RNA, allowed to develop for 6–12 h, fixed in 4% paraformaldehyde for 30 min, rinsed in PBS and tested for photoactivation using the same conditions as described for live embryos.

Antibody staining of Oct4 and Sox17 and quantification of Oct4 protein levels. We compared the expression levels of total Oct4 protein (both paGFP-tagged and endogenous) by antibody staining. Embryos were fixed in 4% paraformaldehyde overnight at 4 °C, rinsed in blocking solution containing 1% bovine serum albumin (BSA) for 20 min at room temperature, incubated with anti-Oct4 goat polyclonal antibodies (Santa Cruz) for 1 h, rinsed again in blocking solution, incubated with donkey anti-goat Alexa-568-conjugated polyclonal antibody (Invitrogen) for 1 h, and rinsed again in PBS. Embryos were imaged immediately following antibody staining. To confirm the correct localization of Sox17 to the nucleus, embryos were fixed in 4% paraformaldehyde overnight at 4 °C, incubated in PBS containing 1% BSA and 0.1%Triton X-100, incubated with NL557-conjugated goat polyclonal anti-Sox17 antibody (R&D Systems) for 1 h, and rinsed again in PBS. Embryos were imaged immediately following antibody staining. We quantified the average fluorescent signal intensity of Oct4 in projections of 5 *z*-planes encompassing entire cell nuclei of injected cells (H2B–RFP labelled) and non-injected cells (H2B–RFP unlabelled; Supplementary Fig. S2a). We confirmed that the antibody recognizes both tagged and untagged Oct4 (data not shown). Because we could photoactivate Oct4–paGFP in ~90% of the cells that expressed H2B–RFP, we assumed that these cells expressed Oct4–paGFP in addition to the endogenous protein. We further tested the functionality of Oct4–paGFP by increasing injection concentration two-fold (4 ng/µl). This manipulation prevented the formation of the blastocoel cavity and presumably also of functional trophectodermal cells by late pre-implantation stages (4.5 dpc; Supplementary Fig. S2c). By contrast, expression of a control H2B–paGFP construct at 4 ng/µl did not have any effect on trophectoderm development. This is in line with a function of Oct4 in antagonizing differentiation of the trophectoderm[43]. It is also in accordance with previous work showing that tagging Oct4 with GFP did not affect its biological function[26]. Comparing total Oct4 levels revealed that the 4 ng/µl concentration increased the average level of total Oct4 expression by approximately 1.8-fold. This further indicates that in the microinjected cells Oct4–paGFP represents the majority of the total Oct4 fraction.

FDAP data analysis. We use a simple model of nuclear import and export of Oct4–paGFP that is similar to the one discussed in ref. 28. We find that Oct4–paGFP kinetics can be captured by the equation

$$\frac{d}{dt}Oct4_n = k_{in}Oct4_c - (k_{out} + k_{deg})Oct4_n \quad (1)$$

Here, $Oct4_n$ is the concentration of mobile Oct4–paGFP in the nucleus and $Oct4_c$ the concentration of Oct4–paGFP in the cytoplasm. The parameters k_{in}, k_{out} and k_{deg} are the rate of Oct4–paGFP import into the nucleus from the cytoplasm, the rate of Oct4–paGFP export from the nucleus to the cytoplasm, and the rate of degradation of Oct4–paGFP, respectively. Besides mobile Oct4–paGFP, there are Oct4–paGFP molecules in the nucleus that are immobile. The dynamics of these Oct4–paGFP molecules are not described by Equation (1) but are captured in a straightforward manner by introducing mobile and immobile fractions μ and $1 - \mu$ of nuclear Oct4–paGFP. Here, $\mu = 1$ corresponds to the extreme situation in which all nuclear Oct4–paGFP is mobile and $\mu = 0$ to the opposite situation in which all nuclear Oct4–paGFP is immobile.

The observed decay of fluorescence intensity in the degradation experiment (Suppl. Fig. S3b) is captured well by the equation

$$f(t) = f_0 e^{-k_{deg}t} \quad (2)$$

which describes the degradation of Oct4–paGFP at rate k_{deg}, where f_0 is the fluorescence intensity at time $t = 0$. We determined k_{deg} by a fit of equation (2) to the experimental data using only k_{deg} as a free fit parameter (Supplementary Fig. S3b).

A key assumption we make is that the kinetics of total Oct4–paGFP (the sum of the fluorescent and non-fluorescent pools) is in steady state. When Oct4–paGFP is photoactivated only in the nucleus, we further assume for simplicity that all Oct4–paGFP imported into the nucleus from the cytoplasm is non-fluorescent (this approach neglects a small fraction of fluorescent Oct4–paGFP that has left the nucleus and can re-enter it). This assumption is plausible because the volume of the cytoplasm is at least two orders of magnitude larger than that of the nucleus and all Oct4–paGFP synthesized *de novo* in the cytoplasm is non-fluorescent. Consistent with this assumption we find that nuclear Oct4–paGFP fluorescence in cells showing the fastest import decreased to values close to zero in our assay (reflected in immobile fractions close to zero in our analysis). This would not happen if a substantial fraction of photoactivated Oct4–paGFP were re-imported into the nucleus. In our analysis, we further assume that the degradation rate of Oct4–paGFP is the same for mobile Oct4–paGFP in the nucleus and in the cytoplasm, whereas immobile Oct4–paGFP is not degraded. This assumption is unproblematic because the degradation rate is small compared with the transport rates and its exact value has only a small effect on the quantification of the export rate. In addition, we assume that the cytosolic Oct4–paGFP concentration is constant during the experiment.

Solving equation (1) for the situation in which only nuclear Oct4–paGFP is photoactivated at $t = 0$ yields an exponential relaxation of the total fluorescence intensity $f(t)$ in the nucleus:

$$f(t) = \mu f_0 e^{-(k_{out}+k_{deg})t} + (1 - \mu)f_0 \quad (3)$$

We used this relation to obtain k_{out} and μ by a fit to the experimental fluorescence intensity data. All fits were performed using Matlab (The Mathworks) function 'fit'. The fit parameters k_{out} and μ were well constrained in all cases.

To obtain the import rate, we activated Oct4–paGFP in the nucleus and in the cytoplasm and quantified the ratio of the nuclear and cytoplasmic Oct4–paGFP concentrations $\frac{Oct4_n^{total}}{Oct4_c}$. Here, $Oct4_n^{total}$ denotes both mobile and immobile Oct4–paGFP in the nucleus and $Oct4_n = \mu \times Oct4_n^{total}$. We found that $\frac{Oct4_n^{total}}{Oct4_c} \approx 10$ in all cells we analysed. We obtained k_{in} using the steady state assumption $\frac{d}{dt}Oct4_n = 0$ in Equation (1):

$$k_{in} = (k_{out} + k_{deg})\mu \frac{Oct4_n^{total}}{Oct4_c} \quad (4)$$

Optimization of photoactivation and effect on the embryo. Photoactivation of paGFP is dependent on the duration of excitation power per unit area. To verify that our irradiation procedure activates the majority of Oct4–paGFP molecules within the nucleus, we performed (in fixed as well as in live embryos) iterated 820 nm photoactivation of Oct4–paGFP in the circular ROI covering 95% of the nucleus. The irradiation wavelength we used was previously shown to be optimal for maximum photoactivation in a fixed developing *Drosophila* wing expressing ubiquitously cytosolic paGFP (ref. 25). The peak intensities of $\leq 9 \times 10^{12}$ W cm^{-2} were held constant during photoactivation. After two to three iterations, full activation could be obtained. At repeated irradiation, photoactivated Oct4–paGFP fluorescence did not increase within the region (Supplementary Fig. S3c). Comparable maximal intensity values of Oct4–paGFP were obtained when photoactivation was performed using 405 nm irradiation with pixel dwell times of less than 4 µs and a maximum available excitation power of ~2 mW at the back aperture of the objective, comparable to previously published excitation settings[25]. Cells in the pre-implantation embryo underwent normal mitosis soon after photoactivation, indicating that our irradiation procedure used in the FDAP experiments activates most of Oct4–paGFP within the nucleus without any phototoxic effect for the mouse embryo.

***z*-fluorescence intensity analysis.** Because most biological tissues scatter light, we assessed its contribution to paGFP fluorescence signal intensity under the same imaging conditions as used during our FDAP assay. For this, we injected *paGFP* RNA into 1-cell stage embryos and photoactivated the entire cell within ROIs localized to several positions along the *z*-axis. We allowed paGFP to spread homogeneously throughout the entire cell for several minutes and then measured its average fluorescence intensity using a line-scanning mode. The results obtained from several cells showed that light scattering could significantly affect fluorescence intensity at distances further than 30 µm away from the focal plane (Supplementary Fig. S3d). We thus restricted our analyses to cells localized within 30 µm along the *z*-axis and excluded from our analyses cells that had shifted their *z* positions significantly during the FDAP assay; this often occurs as a result of spinning of embryos within their surrounding zona pellucida[9].

Photobleaching analysis: To test whether photobleaching during the time-lapse imaging of the FDAP assay could contribute to the decrease of photoactivated Oct4–paGFP fluorescence signal within the cell nucleus, we designed an experiment in which Oct4–paGFP is photoactivated within the cell nucleus and imaged continuously (Supplementary Fig. S3a). Here the nucleus was exposed in <2–5 min to the same number of iterations with the same laser power as in the 4 h FDAP experiments. Quantification of nuclear fluorescence intensity within the cell nucleus revealed that photobleaching contributes less than 2% to overall fluorescence decrease in the cell nucleus. Given the very small value, photobleaching effects can be neglected throughout our experiments.

Linear relation of fluorescence intensity and concentration. To verify a linear relationship between concentration and fluorescence intensity for accurate FDAP assay analysis, we imaged defined concentrations of recombinant GFP in solution for fluorescence/concentration calibration. Different concentrations of recombinant GFP (BioVision Inc.) solution in KSOM + AA medium (Millipore; MR-106-D) were imaged in the same imaging conditions as the FDAP experiments. Individual *z*-sections were used to measure the average fluorescence corresponding to each concentration. The number of GFP molecules corresponding to each GFP concentration was calculated from the sample volume imaged. The sample volume was estimated from the dimensions of the imaged ROI and the thickness of the optical slice using the algorithm in the Zeiss LSM 510. The resulting curves relating the detected fluorescence intensity to the number of GFP molecules (Supplementary Fig. 3d) shows that, below an average fluorescence intensity of approximately 200 counts per pixel, the relationship between concentration and fluorescence intensity is linear. The average fluorescence intensity in the circular ROI covering 95% of the nucleus is below this value, indicating that imaging in the FDAP assay was performed within the linear range of detection.

Statsitics. Description of statistics for Fig. 4c is in caption of Table 2. For the rest, we performed two-tailed Student's *t*-tests assuming unequal variances.

38. Niwa, H., Yamamura, K. & Miyazaki, J. Efficient selection for high-expression transfectants with a novel eukaryotic vector. *Gene* **108**, 193–199 (1991).
39. Boer, B., *et al.* Elevating the levels of Sox2 in embryonal carcinoma cells and embryonic stem cells inhibits the expression of Sox2:Oct-3/4 target genes. *Nucleic Acids Res.* **35**, 1773–1786 (2007).
40. Nowling, T. K., Johnson, L. R., Wiebe, M. S. & Rizzino, A. Identification of the transactivation domain of the transcription factor Sox-2 and an associated co-activator. *J. Biol. Chem.* **275**, 3810–3818 (2000).
41. Zacharias, D. A., Violin, J. D., Newton, A. C. & Tsien, R. Y. Partitioning of lipid-modified monomeric GFPs into membrane microdomains of live cells. *Science* **296**, 913–916 (2002).
42. Sohn, J., *et al.* Identification of Sox17 as a transcription factor that regulates oligodendrocyte development. *J. Neurosci.* **26**, 9722–9735 (2006).
43. Niwa, H., *et al.* Interaction between Oct3/4 and Cdx2 determines trophectoderm differentiation. *Cell* **123**, 917–929 (2005).

ERRATUM

Oct4 kinetics predict cell lineage patterning in the early mammalian embryo

Nicolas Plachta, Tobias Bollenbach, Shirley Pease, Scott E. Fraser and Periklis Pantazis

Nat. Cell Biol. **13,** 117–123 (2011); published online 23 January 2011; corrected after print 28 January 2011;

In the version of this article initially published online and in print, the values for k_{out} and k_{in} in table 1 were incorrect. The correct values are ($\times 10^{-3}\,s^{-1}$). This error has been corrected in both the HTML and PDF versions of the article.

nature cell biology

DOI: 10.1038/ncb2154

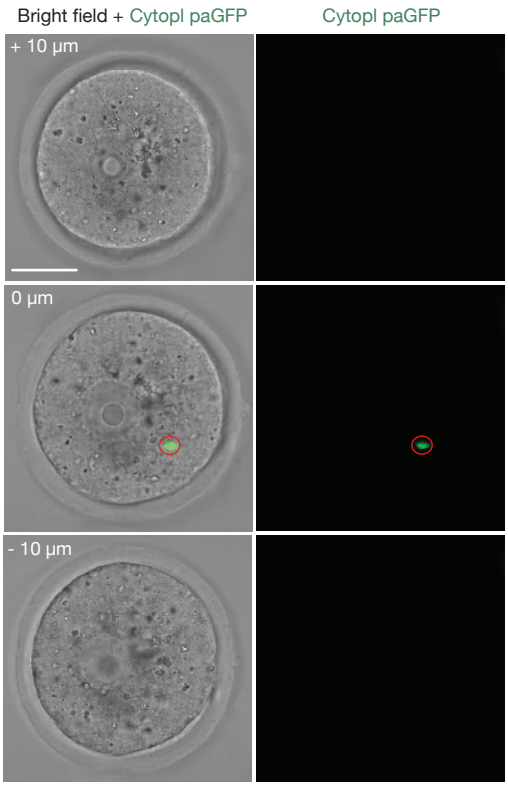

Figure S1 Photoactivation of paGFP in a fixed mouse embryo. A one-cell stage embryo was microinjected with cytoplasmic paGFP RNA and fixed 4 hours after injection in paraformaldehyde. A small ROI (red circle) was photoactivated at a single z-plane. Immediately after photoactivation paGFP fluorescence is confined to the ROI. Fluorescence is not observed at z-planes localized 10 µm above or below the plane of photoactivation (0 µm). Scale bar corresponds to 20 µm.

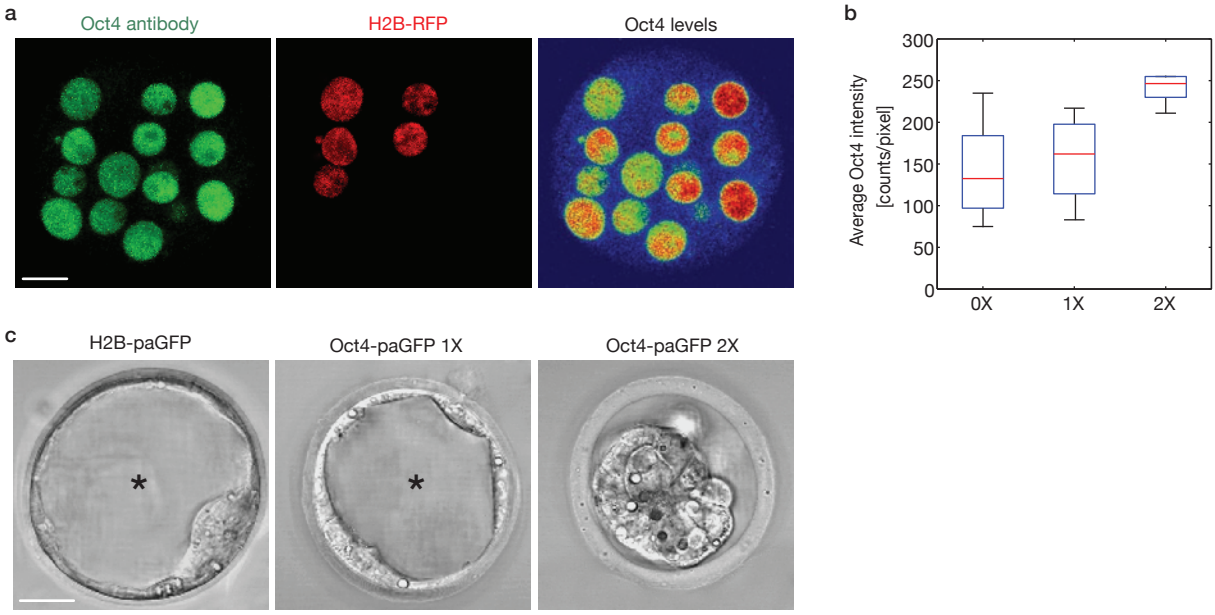

Figure S2 Oct4 expression levels and distribution in mouse embryos. **a**, Oct4 antibody staining shows mostly nuclear localization of Oct4 in z-plane projections encompassing entire cell nuclei. Throughout our study, one cell of the 2-cell stage embryo was microinjected with Oct4-paGFP (2 ng/µl) DNA and H2B-RFP RNA, respectively. All daughter cells derived from the original injected cell are marked by H2B-RFP in their chromatin (red). Note that in the injected H2B-RFP-positive cells total Oct4 expression (green) is similar to that in non-injected H2B-RFP-negative cells. **b**, Boxplot of quantified Oct4 expression levels. At 2 ng/µl (the 1X concentration used in the FDAP experiments) Oct4 is expressed within the physiological range of endogenous Oct4 (0X). At 4 ng/µl (2X) there is a ~1.8-fold increase in Oct4 levels, and the median expression value (red line in graph) is outside the physiological range. **c**, Effects of Oct4-paGFP expression on embryo development. Embryos injected with 2 ng/µl of photoactivatable Oct4-paGFP develop normally to blastocyst stage and form the blastocoel cavity (asterisk). At 4 ng/µl (2X) Oct4-paGFP affects embryonic development and the blastocoel cavity is not formed. A control H2B-paGFP construct injected at 4 ng/µl does not affect embryo development. Scale bar corresponds to 15 µm.

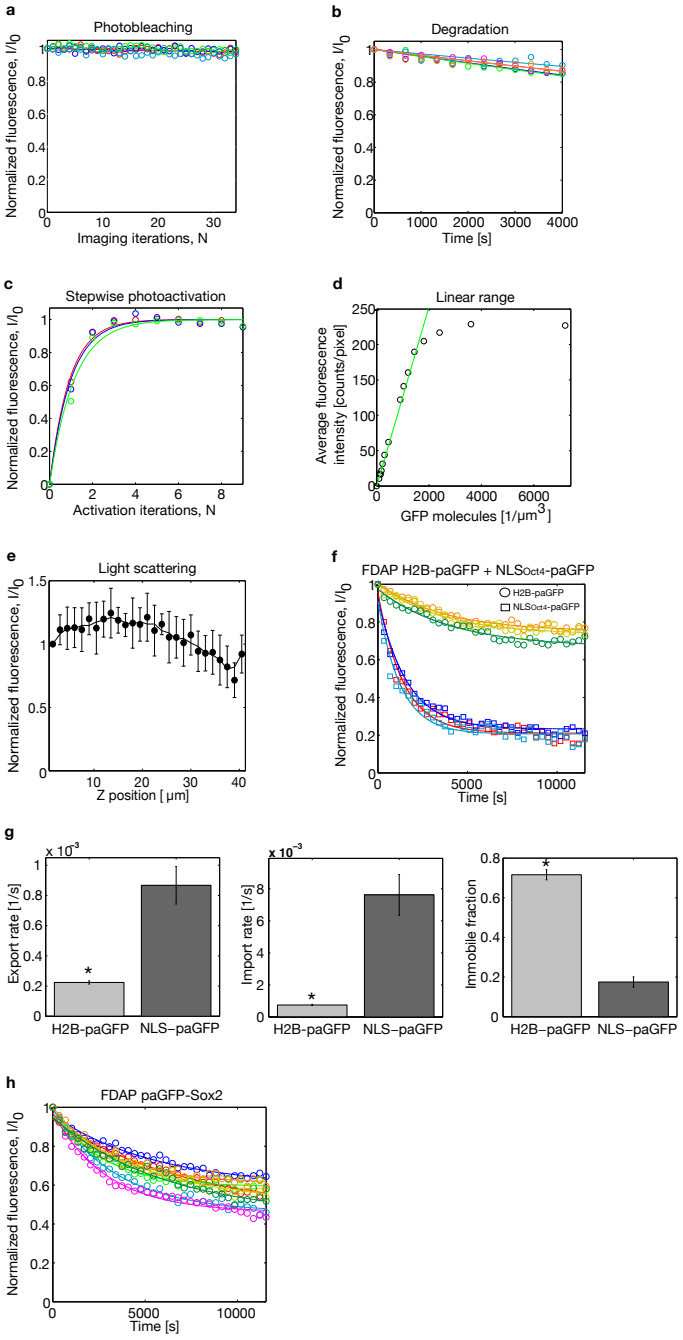

Figure S3 Control experiments for the FDAP assay. **a**, Bleaching in the course of imaging. The contribution of photobleaching by the imaging beam was determined by continuous imaging of Oct4-paGFP fluorescence within a single photoactivated ROI localized to the cell nucleus. **b**, Degradation of photoactivated Oct4-paGFP within the entire cell. Both the cell nucleus and the entire cytoplasm of single cells were photoactivated and the average fluorescence intensity in the whole cell was quantified over time. **c**, Stepwise photoactivation. Photoactivation of Oct4-paGFP in single cell nuclei shows that 2-3 illumination iterations are sufficient to obtain a maximum fluorescence intensity value within the cell nucleus. **d**, Calibration of fluorescence intensity to GFP concentration. GFP in solution at different concentrations was imaged under the same conditions as in the FDAP assay. Three independent measurements for each concentration are shown. A linear regression fit to the first 11 data points is represented by a green line. **e**, Light scattering effect in live mouse embryos. Embryos were microinjected with cytoplasmic paGFP and the average fluorescence intensity was quantified at different z-planes following photoativation of the entire embryo. Light scattering starts affecting fluorescence intensity at ≥ 30 μm distance to the initial focal plane. **f**, FDAP analysis of H2B-paGFP and NLS_{Oct4}-paGFP. H2B-paGFP or NLS_{Oct4}-paGFP were microinjected into 1 cell at the 2-cell stage, photoactivated within single cell nuclei at the 8-cell stage and imaged with the same conditions described for Oct4-paGFP. **g**, Quantification of H2B-paGFP and NLS_{Oct4}-paGFP nuclear export, import and immobile fraction. **h**, FDAP analysis of paGFP-Sox2. paGFP-Sox2 was microinjected into 1 cell at the 2-cell stage, photoactivated within single cell nuclei at the 4- to 8-cell stage and imaged with the same conditions described for Oct4-paGFP. Asterisks show statistically significant differences. Error bars show standard deviations.

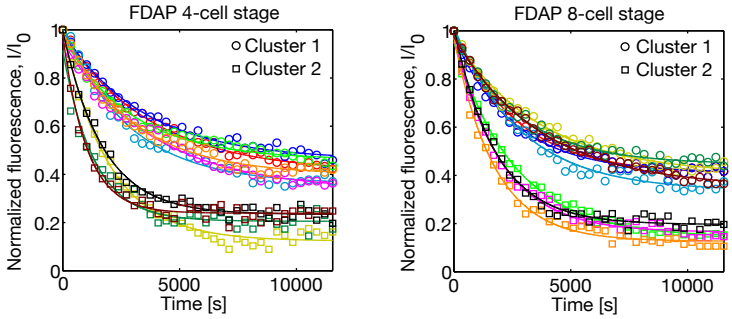

Figure S4 Oct4-paGFP kinetic behaviors at the 4-cell stage and 8-cell stage. FDAP curves for Oct4-paGFP obtained from several cell nuclei of pre-compaction embryos at 4-cell stage (left graph) and at 8-cell stage (right graph). At both developmental stages, cells exhibit two distinct kinetic behaviors, divided into cluster 1 and 2.

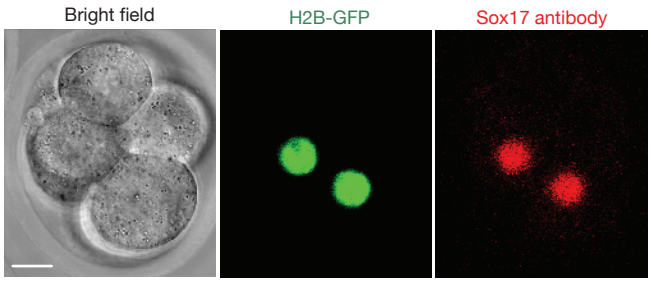

Figure S5 Control experiment for Sox17 expression. In this control experiment, one cell of the 2-cell stage embryo was microinjected with Sox17 (50 ng/μl) RNA and H2B-GFP (10 ng/μl) RNA. All daughter cells derived from the original injected cell are marked by H2B-GFP (green) and exhibit Sox17 protein (red) that localized predominantly in the nuclei. Scale bar corresponds to 15 μm.

Supplementary Movie legends

Movie S1 Selective photoactivation of Oct4-paGFP in a live mouse embryo. Three dimensional view and animated 180° rotation of an 8-cell stage embryo before and after photoactivation of Oct4-paGFP within a single cell nucleus. The appearance of a red circle indicates the ROI photoactivated with 820 nm light. The bright field and the H2B-RFP label show the position of cells in the embryo that express photoactivatable Oct4 before and after photoactivation. Note that photoactivated Oct4 is confined to the cell nucleus immediately after photoactivation.

Movie S2 Imaging Oct4-paGFP in single cells. Time-lapse imaging of two representative photoactivated cell nuclei obtained from a typical FDAP experiment. The cell nuclei belong to two different cells of a pre-compaction, 8-cell stage embryo. The time-lapse sequence was made from a projection of 5 individual z-planes encompassing each cell nucleus. The two nuclei were aligned for comparison. The nucleus on the left panel exhibits the Oct4-paGFP kinetic behavior characteristic of cells in cluster 1, while the nucleus on the right panel displays the behavior of cluster 2 cells.